Journal of Molecular Graphics and Modelling 37 (2012) 59–66

Contents lists available at SciVerse ScienceDirect

Journal of Molecular Graphics and Modelling

journal homepage: www.elsevier.com/locate/JMGM

Calculating the Na^+ translocating V-ATPase catalytic site affinity for substrate binding by homology modeled NtpA monomer using molecular dynamics/free energy calculation

Zahed Muhammed [a], Satoshi Arai [a], Shinya Saijo [a], Ichiro Yamato [a], Takeshi Murata [c], Atsushi Suenaga [b,*]

[a] Department of Biological Science and Technology, Tokyo University of Science, 2641 Yamazaki, Noda-shi, Chiba 278-8510, Japan
[b] Computational Biology Research Center (CBRC), National Institute of Advanced Industrial Science and Technology (AIST), 2-4-7 Aomi, Koto-ku, Tokyo 135-0064, Japan
[c] Department of Chemistry, Graduate School of Science, Chiba University, 1-33Yayoi-cho, Inage, Chiba 263-8522, Japan

ARTICLE INFO

Article history:
Received 11 October 2011
Received in revised form 25 February 2012
Accepted 10 March 2012
Available online 30 March 2012

Keywords:
V-ATPase
Nucleotide binding
Molecular dynamics
Free energy calculation
Homology modeling

ABSTRACT

Vacuolar ATPase (V-ATPase) of *Enterococcus hirae* is composed of a soluble catalytic domain (V_1; $NtpA_3$-B_3-D-G) and an integral membrane domain (V_o; NtpI-K_{10}) connected by a central and two peripheral stalks (NtpC, NtpD-G and NtpE-F). Recently nucleotide binding of catalytic NtpA monomer has been reported (Arai et al. [19]). In the present study, we calculated the nucleotide binding affinity of NtpA by molecular dynamics (MD) simulation/free energy calculation using MM-GBSA approach based on homology modeled structure of NtpA monomer docked with ATP analogue, adenosine 5′-[β, γ-imido] triphosphate (AMP-PNP). The calculated binding free energies showed qualitatively good agreement with experimental data. The calculation was cross-validated further by the rigorous method, thermodynamic integration (TI) simulation. Finally, the interaction between NtpA and nucleotides at the atomic level was investigated by the analyses of components of free energy and the optimized model structures obtained from MD simulations, suggesting that electrostatic contribution is responsible for the difference in nucleotide binding to NtpA monomer. This is the first observation and suggestion to explain the difference of nucleotide binding properties in V-ATPase NtpA subunit, and our method can be a valuable primary step to predict nucleotide binding affinity to other subunits (NtpAB, $NtpA_3B_3$) and to explore subunit interactions and eventually may help to understand energy transduction mechanism of *E. hirae* V-ATPase.

1. Introduction

Na^+ translocating vacuolar type ATPase (V-ATPase) is a variant of proton pumping V-ATPase family [1]. It was found in a Gram positive fermentative bacterium *Enterococcus hirae* and found to translocates Na^+ in expense of ATP hydrolysis [2]. It is a multi-subunit enzyme consisting of a hydrophilic catalytic portion (V_1; $NtpA_3$-B_3-D-G) and a membrane-embedded portion (V_o; NtpI-K_{10}) connected by a central and two peripheral stalks (NtpC and NtpE-F). Energy transfer between ATP hydrolysis and Na^+ movement requires three catalytic sites in the catalytic moiety (V_1) and Na^+ translocating proteolipid in the membrane embedded portion (V_o) (see model in Fig. 1).

Adenosine triphosphate synthase (ATP synthase, F_oF_1-ATPase), which can also hydrolyse ATP, has structural similarity with V-ATPase [1,3]. It also has three catalytic β subunits which corresponds to catalytic A subunits of V-ATPase. Research on F_oF_1-ATPase has been much ahead of V-ATPase research and central metabolic role as well as high efficiency of this machine has triggered much experimental work on substrate binding [4], stoichiometry [5], three dimensional structures [6], single molecule observation [7], and kinetics [4], as well as on mutants [8]. Recently molecular dynamics (MD) simulation/free energy calculation study has been successfully applied to understand the detailed mechanism of this enzyme when biochemical or structural studies were not sufficient to answer questions about energy transduction in relation to conformational change, ATP hydrolysis or synthesis [9–13]. These studies explained the vital link between ligand binding affinities to the different structural conformations of catalytic subunits [9].

In case of *E. hirae* V-ATPase, although extensive biochemical studies [14–21] as well as crystal structure of integral membrane domain (V_o) has been reported [22], computer simulation studies have not yet been applied, since we do not have the high resolution crystal structure of the catalytic V_1 moiety of this intriguing

* Corresponding author. Tel.: +81 3 3599 8913; fax: +81 3 3599 8081.
E-mail addresses: atsushi.suenaga@aist.go.jp, suenaga1214@gmail.com (A. Suenaga).

1093-3263/$ – see front matter © 2012 Elsevier Inc. All rights reserved.
http://dx.doi.org/10.1016/j.jmgm.2012.03.006

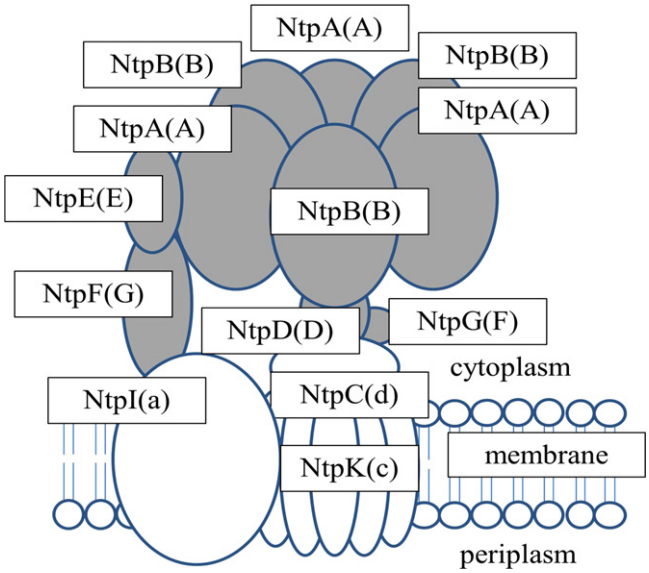

Fig. 1. Schematic model of *E. hirae* V-ATPase. The names of the corresponding subunits of eukaryotic V-ATPase are in parentheses. In this study homology model of NtpA (catalytic subunit) was constructed and AMP-PNP was docked for molecular dynamic/free energy calculation study.

enzyme. But the crystal structure of A subunit of A-ATP synthase from *Pyrococcus horikoshii* OT3 [23] have been published. Thus we started MD/free energy calculation using homology modeled structure of *E. hirae* A subunit. We have published reconstitution study of V_1 portion of V-ATPase with catalytic NtpA monomer, non-catalytic NtpB monomer and NtpDG heterodimer purified by using *Escherichia coli* expression system *in vivo* or *in vitro* [19]. The affinity (K_D) of nucleotide binding to catalytic subunit NtpA was 6.6 μM for ADP and 3.1 μM for ATP [19].

We compared the calculated free energy difference with the obtained experimental data to establish reliable free energy calculation methodology to apply on *E. hirae* V-ATPase. This serves as the first model study of *E. hirae* V-ATPase simulation and helps us to apply similar methods to understand detailed mechanism of this fascinating enzyme at atomic level details. Currently structure determination by X-ray crystallography of V_1 moiety and different subunits of V_1 moiety of *E. hirae* V-ATPase is under process out in our laboratory. Applying the established method in this report to the whole V_1 moiety, we expect to answer vital questions of free energy change during ATP hydrolysis cycle and shed lights on the overall energy transduction of the enzyme.

2. Materials and methods

2.1. Homology modeling of NtpA monomer

The amino acid sequence of NtpA monomer of V-ATPase was retrieved from the NCBI database (Acc. no. BAA04275) and used to search non redundant protein chains from the Protein Data Bank (PDB) *via* NCBI-BLAST using BLOSUM62 scoring matrix in Discovery Studio software package version 2.5.5 (Accelrys Inc., San Diego, CA). The crystal structure of the catalytic subunit A of A-type ATPase from *P. horikoshii* OT3 (PDB: 1VDZ) and the crystal structure of the A_3B_3 complex of V-ATPase from *Thermus thermophilus* (PDB: 3GQB) were ultimately selected as templates due to their relatively close sequence identity and functional similarity. After successful sequence alignment, NtpA monomer was modeled against two templates (PDB: 1VDZ and 3GQB) using modeler [24] *via* Discovery Studio 2.5.5. The loops were refined using modeler energy function and the refined model was validated using "Profile 3D verify" by the same software package mentioned above.

2.2. Computational docking of AMP-PNP

The homology model of NtpA monomer created above was used for AMP-PNP docking studies using Discovery Studio software package version 2.5.5. Briefly, AMP-PNP including Mg^{2+} was extracted from crystal structure of F_1-ATPase (PDB: 1BMF) for docking purpose. Amino acid residues around the typical ATP-binding site (P-loop) of modeled NtpA monomer were selected and a ligand sphere was defined surrounding these residues. AMP-PNP was then docked using CDOCKER [25] in Discover Studio 2.5.5. CDOCKER is a CHARMm-based molecular dynamics (MD) method for ligand docking. In current study, 10 random conformations of docked nucleotide (AMP-PNP) were generated. After these conformations were translated to binding sphere, candidate poses were created using random-rigid body rotations followed by simulated annealing and a final energy minimization. Each candidate AMP-PNP pose on the NtpA monomer was scored using a default scoring function *i.e.* "-CDOCKER energy". The best NtpA-AMP-PNP complex was selected based on "-CDOCKER energy" for free energy calculation purpose.

2.3. System setup

Initial structures for molecular dynamics (MD) simulation/free energy calculation was homology modeled NtpA-AMP-PNP (NtpA monomer docked with AMP-PNP). For MM-GBSA study, NtpA-ATP and NtpA-ADP were created by manipulating the atoms in the above mentioned original NtpA-AMP-PNP PDB file. To neutralize the net charge of the simulation system, counter ions (Na^+) were added by using the Leap module in the Amber program package. Partial charges for the ligands, which were not included in the standard parm96 parameter set, were calculated at RHF/6-31G*//B3LYP/cc-pVTZ SCRF level with Gaussian98 and the restrained electrostatic potential (RESP) method [26]. The parameters for the ligands were determined using the antechamber module version 1.27 of AMBER 8.0 by utilizing the general atom force field (GAFF).

All figures in the present study were prepared with the VMD graphics programs [27] and Discovery Studio 2.5.5. All simulations were performed using RICC (RIKEN Integrated Clusters of Computers) of RIKEN (The Institute of Physical and Chemical Research) Yokohama, Japan.

The complexes (NtpA-AMP-PNP, NtpA-ATP, NtpA-ADP) were energy minimized in order to remove possible steric stress by multi step procedures. First, water molecules were allowed to relax while the rest of the system was kept frozen. The steepest decent methods (1000 steps) followed by the conjugated gradient (2500 steps) were used. Second, all atoms of the complex were relaxed together with water molecules (25,000 steps) and a final energy gradient was achieved for all the systems which was reasonable gradients for local minimum for each system.

2.4. Molecular dynamics simulation

In all calculations described in the present study, Amber *ff03* force field as implemented with AMBER 10 suite of programs was adopted. The solvent was considered explicitly with TIP3P-point charge model. All simulations were carried out under periodic boundary conditions.

MD simulation was initiated by heating the minimized structures from 0 K to 300 K over a period of 40 ps with the protein atom being kept frozen. Finally, 2 ns dynamic calculation was performed in the NTP ensemble, keeping the pressure constant at 1 atm and

constant temperature of 300 K using Berendsen's thermostat [28]. All calculations were performed using Amber version 10 at RICC (RIKEN Integrated Cluster of Clusters) system with a time step of integration set to 2 fs. The bond lengths involving hydrogen atoms were constrained to equilibrium lengths using SHAKE method [29]. Electrostatic interactions were treated with particle mesh Ewald method with a cut-off of 10 Å.

2.5. Free energy calculation using the MM-GBSA method

Theoretical binding free energies were calculated within the one-trajectory protocol using the MM-GBSA (Molecular Mechanics-Generalized Born Surface Area) approach [30] described as:

$$\Delta G_{\text{binding}} = G_{\text{complex}} - (G_{\text{receptor}} + G_{\text{ligand}})$$

$$G_{\text{molecule}} = \langle E_{\text{gas}} \rangle + \langle G^{\text{polar}}_{\text{solvation}} \rangle + \langle G^{\text{nonpolar}}_{\text{solvation}} \rangle - \text{TS}$$

$$\langle E_{\text{gas}} \rangle = \langle E_{\text{internal}} \rangle + \langle E_{\text{electrostatic}} \rangle + \langle E_{\text{vdW}} \rangle$$

$$G^{\text{nonpolar}}_{\text{solvation}} = \gamma\,\text{SASA}$$

The production MD trajectory was collected for a 500 ps period (from 1500 to 2000 ps) with each snapshot saved every 5 ps. The set of structures obtained from MD trajectory was sampled for use in estimating binding free energies. In the analysis of the binding free energies, the water molecules were replaced with implicit solvation model. $\langle\,\rangle$ denotes the average value of the selected set of structures along the molecular dynamics trajectory. Internal energy (E_{internal}) includes bond, angle and dihedral energies, and $E_{\text{electrostatic}}$ and E_{vdW} are intermolecular electrostatic and van der Waals energies, respectively. All these terms were calculated by molecular mechanics *in vacuo*. Electrostatic contribution to the free energy of solvation ($G^{\text{polar}}_{\text{solvation}}$) was calculated by a continuum representation of the solvent within the Generalized Born model and non-polar contribution to solvation ($G^{\text{nonpolar}}_{\text{solvation}}$) was obtained by using a simple linear relationship with the SASA (Solvent Accessible Surface Area), where γ gets the value of 0.0072 kcal/mol Å^2.

2.6. Thermodynamic integration

The equation that relates the free energy of binding (ΔG) to K_D is: $\Delta G = -RT \ln K_D$. To calculate the relative binding free energy of nucleotide to different subunits we used following thermodynamic cycle:

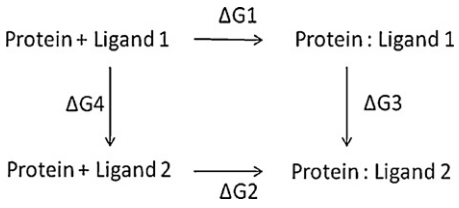

Here, the change from ligand1 to ligand2 represents change of AMP-PNP to ATP or ATP to ADP and protein represents homology modeled NtpA monomer either in solution or in complex with any nucleotide (AMP-PNP, ATP or ADP). Because this thermodynamic cycle is closed, the equality, $\Delta G1 + \Delta G3 = \Delta G2 + \Delta G4$, can be held. Here, $\Delta G1$ and $\Delta G2$ values can be obtained experimentally. Whereas, $\Delta G4$ or $\Delta G3$ represents AMP-PNP to ATP or ATP to ADP free energy changes in solution as well as in complex, respectively, which can be calculated by molecular dynamics (MD) simulation/free energy calculation. The relative binding free energy can be calculated as $\Delta\Delta G_{2\rightarrow 1} = \Delta G1 - \Delta G2 = \Delta G4 - \Delta G3$. To compute $\Delta G4$ and $\Delta G3$, we used TI method [31]. The snapshot at 2 ns obtained from MD simulation was used as the initial structure for the TI simulation. In TI calculations, above transformations are broken up into three sub steps when using AMBER 10 module. These are (1) charge change, (2) vdW-transformation, and (3) atomic partial charge addition to newly added atoms. The partial charges of atoms are gradually increased (or decreased) in seven steps (windows) increasing the coupling parameter, *clambda*, from 0 to 1, and van der Waals parameters of atoms are gradually increased (or decreased) in nine steps (windows) increasing *clambda* from 0 to 1. During the change of vdW, soft-core potential was activated (by setting ifsc = 1). The system in each window was simulated for 250 ps (simulation protocol was the same as that of MD simulation) and the last 50 ps of data were used for the calculation of $\langle \partial H/\partial\lambda \rangle = dG/d\lambda$. From Gaussian quadrature formulas of higher order, ΔG is approximately calculated as $\Delta G \approx \sum w_i \langle \partial H/\partial\lambda \rangle_{\lambda i}$. The combination of w_i and λ_i used in this study is given in Table 3.

3. Results and discussion

3.1. Homology model of NtpA monomer

A search of non-redundant protein structures in the current release of Protein Data Bank (PDB) *via* NCBI-BLAST yielded several homologues of NtpA subunit of V-ATPase. By sequence alignment of NtpA of *E. hirae* to A-subunits of *P. horikoshii* OT3 and *T. thermophilus* altogether showed 35.7% sequence identity and 55.4% sequence similarity (Fig. 2A). We chose these two candidates for our homology modeling because these are similarly homologous to our query sequence but not highly similar to each other. Thus, the query sequence may align better to one template at one region and to another at another region. Finally, the overall fold of our homology model of NtpA monomer was typical of V-ATPase catalytic subunit [32]. Superimposition of main chain atoms from NtpA of *E. hirae* and A subunit of *T. thermophilus* showed close similarity, with root mean square deviation (RMSD) of only 2.384 Å (Fig. 2B).

3.2. AMP-PNP binding to NtpA monomer

NtpA should have the nucleotide-binding site as the catalytic subunit, which has typical Walker-A motif (GXXGXGKTV). The area forming this Walker-A motif was used to determine the positioning of nucleotide binding sphere in *in silico* docking. The sphere was centered at this area (P-loop) with a radius of about 15 Å. The program CDOCKER was used for docking and the highest scoring pose was selected. Major residues known [32,33] to bind nucleotide at catalytic site are in close proximity of the phosphate moiety of docked AMP-PNP (Fig. 3). The modeled structure with nucleotide was close to the reported structure of V-ATPase A-subunits having bound AMP-PNP [32].

3.3. Free energy analysis by MM-GBSA

We applied the MM-GBSA to calculate the binding free energy of the NtpA-AMP-PNP, NtpA-ATP and NtpA-ADP complexes binding AMP-PNP, ATP and ADP, respectively. Structures of NtpA-ATP and NtpA-ADP complexes were prepared from NtpA-AMP-PNP complex as described in Section 2. Table 1 shows the relevant data (in kcal/mol units) from MM-GBSA analysis using above complexes. By comparing each component of free energy, one can find that the similar recognition interaction works between NtpA and AMP-PNP or ATP but the recognition mechanism is different for ADP. This is expected, since ADP lacks γ-phosphate in its phosphate strings so that the net charge of ADP was different from that of AMP-PNP and ATP. However, the sum of these components, total binding free

Fig. 2. (A) Alignment of the amino acid sequences of NtpA subunit of *Enterococcus hirae*, A-subunit of *Pyrococcus horikoshii* OT3 (PDB: 1VDZA) and A-subunit of V-ATPase from *Thermus thermophilus* (PDB: 3GQBA). Dark blue indicates identical residues and light blue indicates similar residues. (B) Cartoon representation of superimposition of homology modeled NtpA of *E. hirae* (yellow) and A subunit of *Thermus thermophilus* (red). (For interpretation of the references to color in this figure legend, the reader is referred to the web version of this article.)

energy ΔG_{calc}, of AMP-PNP was different from that of ATP and ADP (Table 1). This indicates that the balance between components was important for the binding free energy.

The binding free energy of all three nucleotides showed good correspondence with experimental data. The binding affinity of ATP to NtpA subunit as shown in Table 1 was higher than those of AMP-PNP and ADP. Interestingly, AMP-PNP, an analogue of ATP, showed lower affinity toward NtpA both in experiment and MM-GBSA analysis (Table 1). The component analysis of MM-GBSA results shows that the most significant difference between NtpA-AMP-PNP and NtpA-ATP is at the electrostatic contribution ($\Delta G_{ele} = \Delta E_{ele} + \Delta G_{sol}{}^{pol}$); which is higher for NtpA-AMP-PNP. In case of NtpA-ADP, electrostatic balance (ΔE_{ele}) is lower and the van der Waals contribution (ΔE_{vdW}) is smaller while the van der Waals contribution (ΔE_{vdW}) are similar for NtpA-AMP-PNP and NtpA-ATP complexes. In this study, the entropy contribution of solute (S) was not calculated. The difference of S among AMP-PNP, ATP and ADP (ΔS) are expected to be small so that the effect of the entropy contribution to a trend of ΔG would be also small. The aim of this study is to predict a trend of ΔG not the absolute ΔG. Due to intrinsic limitation of the method [34] absolute binding free energies are overestimated.

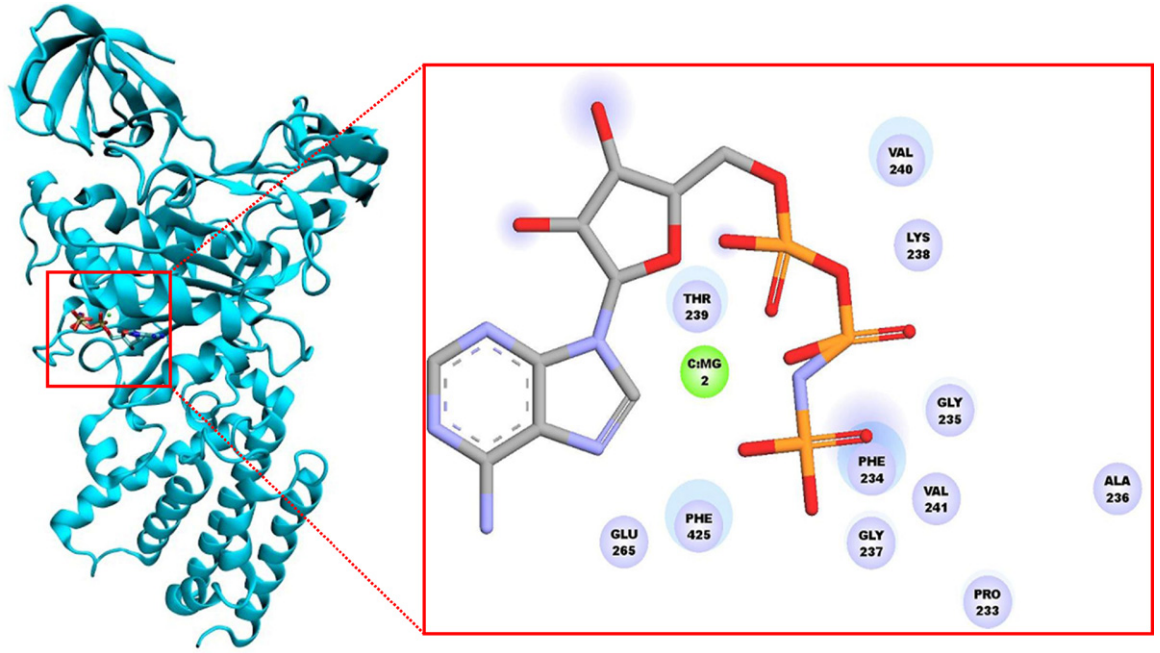

Fig. 3. Binding of AMP-PNP to homology modeled NtpA of *E. hirae*. The zoom-in window shows the AMP-PNP successfully docked in the expected P-loop region of the modeled NtpA monomer. A blue halo around some of the residues represents the solvent accessible surface.

Table 1
Summary of MMGBSA results.

	NtpA-AMP-PNP	NtpA-ATP	NtpA-ADP
ΔE_{ele}	598.91	542.35	181.06
ΔE_{vdW}	−43.02	−46.71	−35.06
ΔE_{Int} [c]	−0.00	−0.00	−0.00
ΔE_{gas} [d]	555.89	495.64	146.00
$\Delta G_{sol}{}^{non\text{-}pol}$	−5.18	−4.75	−4.50
$\Delta G_{sol}{}^{pol}$	−560.94	−522.88	−165.32
ΔG_{sol} [e]	−566.12	−527.62	−169.82
ΔG_{ele} [f]	37.97	19.48	15.74
ΔG_{calc}	−10.24	−31.98	−23.82
ΔG^{exp}	−4.53[a]	−7.56[b]	−7.11[b]

Binding free energy was calculated by averaging 100 snapshots for the studied complexes. All values are shown in kcal/mol units. ΔE_{ele} and ΔE_{vdW} account for the electrostatic and van der Waals *in vacuo* binding enthalpic contribution. $\Delta G_{sol}{}^{non\text{-}pol}$ accounts for the non-polar contribution to solvation, $\Delta G_{sol}{}^{pol}$ is the polar contribution in solvation. ΔG_{sol} denotes for the $\Delta G_{sol}{}^{non\text{-}pol} + \Delta G_{sol}{}^{pol}$. ΔG_{ele} accounts for the $\Delta E_{ele} + \Delta G_{sol}{}^{pol}$ addition. $\Delta G_{calc} = \Delta E_{gas} + \Delta G_{sol}$ accounts for the sum of polar and non-polar solvation contribution to binding free energy.

[a] From affinity constant of Arai et al. (unpublished data).
[b] From affinity constant of Arai et al. [19].
[c] ΔE_{Int} = bond, angle, dihedral energies.
[d] $\Delta E_{gas} = \Delta E_{Int} + \Delta E_{ele} + \Delta E_{vdW}$.
[e] $\Delta G_{sol} = \Delta G_{sol}{}^{non\text{-}pol} + \Delta G_{sol}{}^{pol}$.
[f] $\Delta G_{ele} = \Delta E_{ele} + \Delta G_{sol}{}^{pol}$.

Table 2
Summary of TI results.

	TI simulation	Free energy difference (ΔG) with error	
Unbound ($\Delta G4$)	AMP-PNP → ATP	192.89 ± 3.78	
	ATP → ADP	266.17 ± 4.53	
Bound ($\Delta G3$)	AMP-PNP → ATP	188.41 ± 3.68	
	ATP → ADP	266.84 ± 5.10	
ΔG_{exp} ($\Delta G1$, $\Delta G2$)	AMP-PNP	ATP	ADP
	−4.53[a]	−7.56[b]	−7.11[b]
$\Delta\Delta G_{ATP \rightarrow AMP\text{-}PNP}{}^{calc}$	+4.48	192.89–188.41	
$\Delta\Delta G_{ATP \rightarrow ADP}{}^{calc}$	+0.58	266.85–266.17	
$\Delta\Delta G_{ATP \rightarrow AMP\text{-}PNP}{}^{exp}$	+3.03	−4.53 to −7.56	
$\Delta\Delta G_{ATP \rightarrow ADP}{}^{exp}$	+0.45	−7.10 to −7.56	

Free energy changes as a result of AMP-PNP changed to ATP and ATP changed to ADP in bound and unbound state (in solution) estimated from TI simulations (kcal/mol) are shown. $\Delta G1$, $\Delta G2$, $\Delta G3$ and $\Delta G4$ are shown according to the thermodynamic cycle as shown in Section 2. Comparison of experimentally obtained free energy difference data ($\Delta\Delta G^{exp}$) and calculated values ($\Delta\Delta G^{calc}$) are presented at the bottom of the table.

[a] From affinity constant of Arai et al. (unpublished data).
[b] From affinity constant of Arai et al. [19].

3.4. Thermodynamic integration (TI)

In addition to MM-GBSA method, we also used TI simulations (see Section 2) to validate the data of MM-GBSA. TI simulations can directly provide free energy difference of binding of nucleotides to NtpA relative to the binding of AMP-PNP. TI simulation is well known as a precise method to calculate $\Delta\Delta G$, and it requires a huge computational costs. In 250 ps simulation, free energy change from AMP-PNP to ATP in unbound state was 192.893 ± 3.78 kcal/mol (Table 2) which is represented by $\Delta G4$ in the thermodynamic cycle (see Section 2). On the other hand, free energy change for AMP-PNP to ATP in NtpA:AMP-PNP complex was 188.410 ± 3.68 kcal/mol (Table 2). This is represented as $\Delta G3$ in the thermodynamic cycle. The free energy difference is

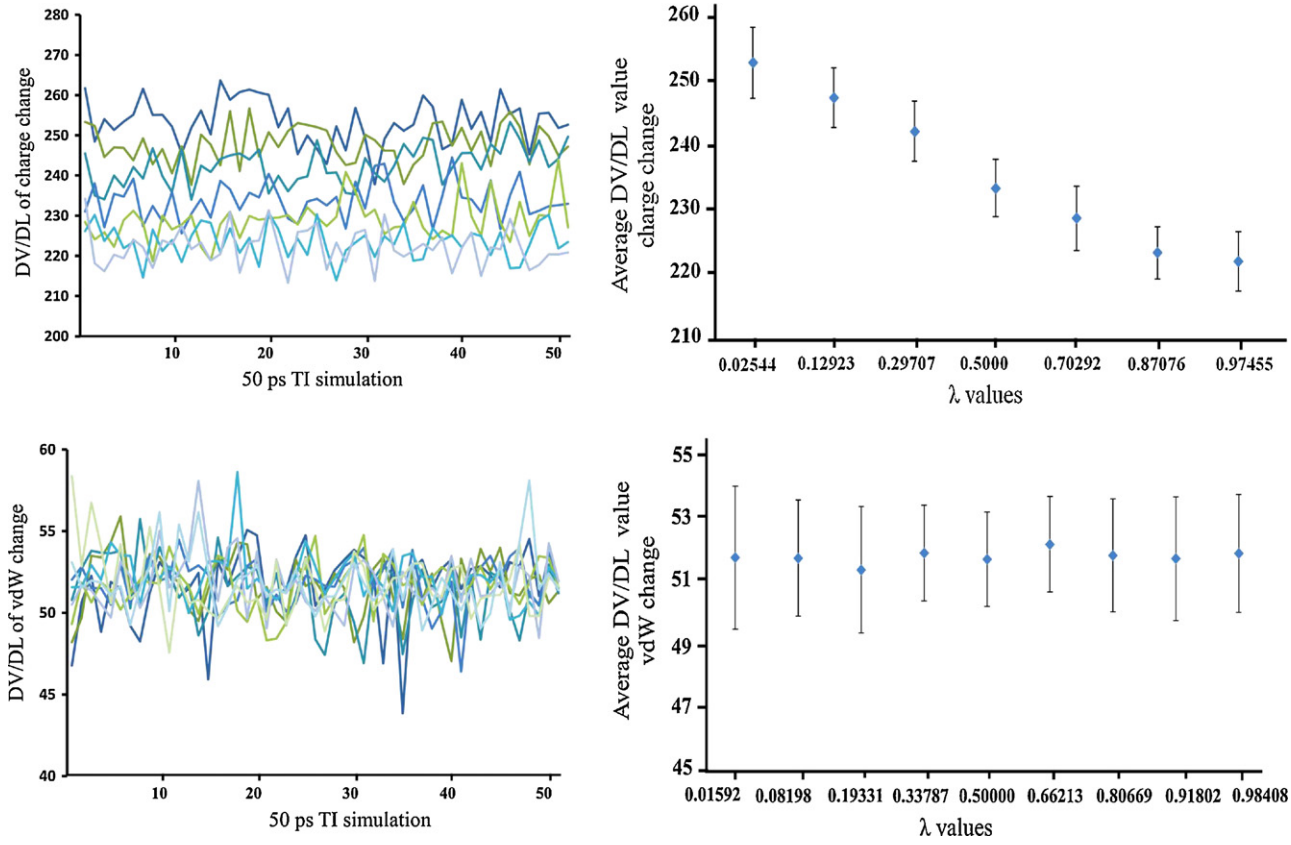

Fig. 4. DV/DL values plotted against 50 ps TI simulation in upper and lower left panels for charge and vdW changes respectively, to demonstrate convergence in homology modeled NtpA subunit with ligand in water environment. The upper and lower right panels show the cumulative averages of DV/DL data as a function of λ during charge change (seven lambda windows) and vdW change (nine lambda windows), respectively.

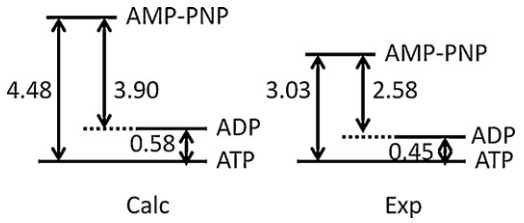

Fig. 5. Schematic representation of the relative free energy differences of binding interactions of NtpA with nucleotides. All values are shown in kcal/mol units.

calculated as $\Delta\Delta G_{2\rightarrow 1} = \Delta G1 - \Delta G2 = \Delta G4 - \Delta G3$. The binding affinity of AMP-PNP and ATP to NtpA was obtained experimentally as −4.53 kcal/mol (unpublished data) and −7.56 kcal/mol [19], which correspond to $\Delta G1$ and $\Delta G2$ in the thermodynamic cycle respectively. According to our TI simulations, we obtained $\Delta\Delta G_{\text{ATP}\rightarrow\text{AMP-PNP}}{}^{\text{exp}} = \Delta G1 - \Delta G2 = -4.53 - (-7.56) = +3.03$ kcal/mol and $\Delta\Delta G_{\text{ATP}\rightarrow\text{AMP-PNP}}{}^{\text{calc}} = \Delta G4 - \Delta G3 = 192.89 - 188.410 = +4.48$ kcal/mol (Table 2). Using similar thermodynamic cycle and our TI calculated data we obtained $\Delta\Delta G_{\text{ATP}\rightarrow\text{ADP}}$ as +0.58 kcal/mol (experimental value +0.45 kcal/mol) (Table 2). The graphs of raw DV/DL data (Fig. 4 and Supplementary Fig. 1A and B) clearly demonstrate the convergence, and the expected ranges of standard deviations (3.7–5.1 kcal/mol) for ΔG were observed, which are quite small (∼2%) comparing to the values of ΔG (Table 2). Although it seems a little high, there will be always higher standard deviation during the charge change step because of larger values of free energy change. In this respect, we think that the calculated data are relatively accurate and reflect the real situation of affinity changes of nucleotide binding. The obtained data also showed excellent agreement with experimental values (Table 2; Fig. 5) and

Table 3
Thermodynamic integration data: abcissas (λ_i) and weights (w_i) for Gaussian integration are shown.

$n = 12$[a]		$n = 9$[a]	
$w_i^{\dagger}$	$\lambda_i^{\ddagger}$	$w_i^{\dagger}$	$\lambda_i^{\ddagger}$
0.06474	0.02544	0.04064	0.01592
0.13985	0.12923	0.09032	0.08198
0.19091	0.29707	0.13031	0.19331
0.20897	0.50000	0.15617	0.33787
0.19091	0.97455	0.16512	0.50000
0.13985	0.87076	0.15617	0.98408
0.06474	0.70292	0.13031	0.91802
		0.09032	0.80669
		0.04064	0.66213

$w_i^{\dagger}$ values were calculated from Eq. (14) in Hummer and Szabo [35].
$\lambda_i^{\ddagger}$ values were calculated from the solutions of Legendre's polynomial.
[a] Number of windows in integration.

corresponded well with the correlation between MMGBSA results and experimental values (Table 3).

3.5. Difference in nucleotide binding to NtpA monomer

AMP-PNP showed the lowest affinity to NtpA monomer in both experiment and calculation. It is interesting to obtain information concerning the nature of interactions of nucleotide and the NtpA monomer that contribute to the free energy values obtained during AMP-PNP to ATP or ATP to ADP change. Such analysis is particularly important, since in spite of the structural similarity, AMP-PNP and ATP showed different values of ΔG and binding affinities toward NtpA monomer: AMP-PNP was a weak binder to NtpA monomer in both experimental and calculated result. This weak binding may be due to the highly positive

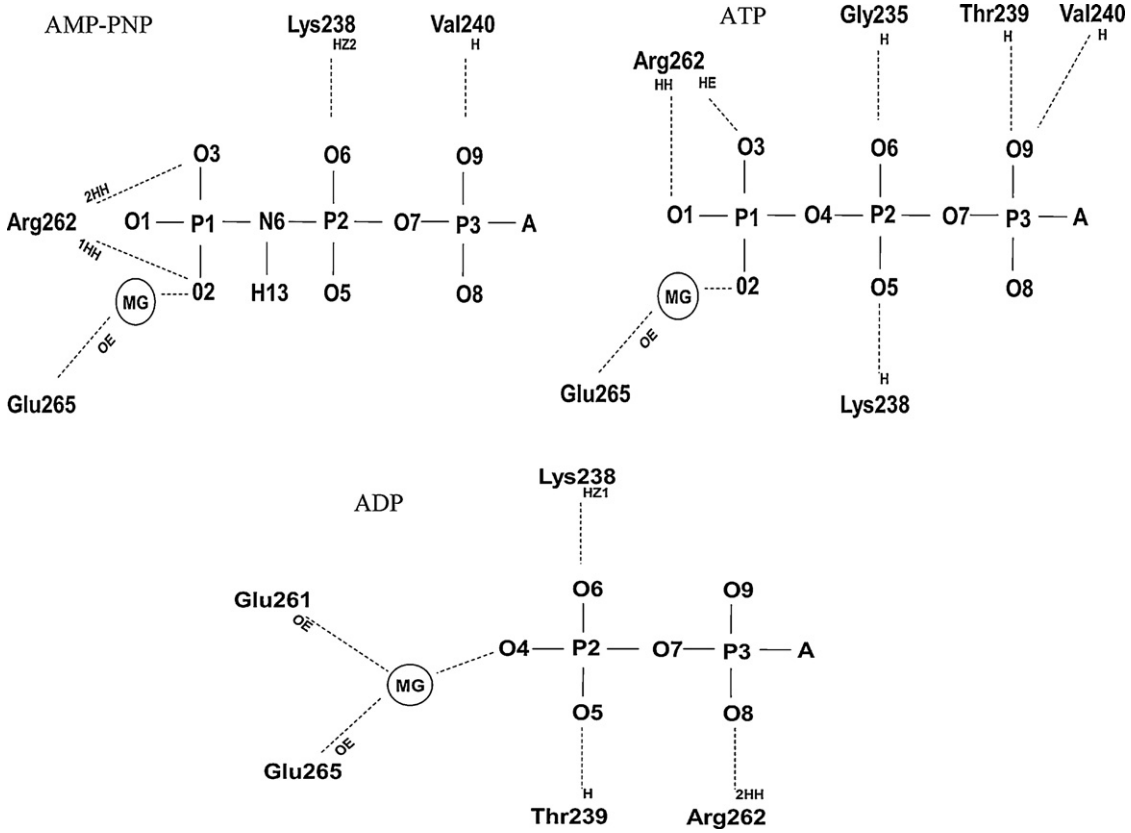

Fig. 6. Schematic representation of NtpA monomer/nucleotide binding interface obtained from MD simulation. Hydrogen (H) atoms of Lys 238, Gly 235, Thr 239 and Val 240 shown in the figure indicate hydrogen atoms of backbone NH group. Interaction of phosphate moiety of nucleotides with NtpA monomer are shown by dashed lines.

electrostatic contribution during binding. In MM-GBSA experiment we found that ΔG_{ele} for AMP-PNP showed highly positive value (37.97 kcal/mol in Table 1). This may make AMP-PNP unstable when in complex with NtpA monomer compared to ATP or ADP. Also in TI experiment, $\Delta\Delta G_{ele}{}^{\text{AMP-PNP to ATP}} = 2.76$ kcal/mol and $\Delta\Delta G_{ele}{}^{\text{ATP to ADP}} = 0.591$ kcal/mol. Therefore, during AMP-PNP to ATP change, electrostatic interaction contributed to instability for the binding AMP-PNP to NtpA monomer. To explore this point further, we analyzed 2 ns equilibrated structures of NtpA-AMP-PNP, NtpA-ATP and NtpA-ADP and explored the nature of interactions between ligand and protein. For interaction analysis, the optimized model structures obtained from MD simulations were analyzed, where we considered a pair is making interactions, when the distance between two atoms was less than 2 Å during 80% of the simulation time. Fig. 6 shows the schematic representation of the electrostatic interaction between nucleotides (AMP-PNP, ATP and ADP) and NtpA monomer. The oxygen (O4) in ATP is replaced with N-H (N6-H13) in AMP-PNP. It caused the conformational change of the phosphate group in the nucleotide hence the binding mode between the phosphate group and NtpA was changed between AMP-PNP and ATP. Two hydrogen bonds were lost in case of AMP-PNP as compared to ATP (Fig. 6, AMP-PNP and ATP). This may be the reason behind the highly positive electrostatic contribution for AMP-PNP binding to NtpA in both MM-GBSA analysis and TI calculation: loss of two hydrogen bond may cause weak binding of AMP-PNP to NtpA monomer compared to ATP. In case of ADP, three hydrogen bonds were lost, which could make ADP unstable for interacting with NtpA monomer but this instability was compensated *via* formation of additional ion pairing between Mg^{+2} and Glu 261(Fig. 6, ADP). As a result, no significant difference in electrostatic contribution was resulted in both TI simulation during ATP to ADP change (0.591 kcal/mol) and MM-GBSA analysis (ΔG_{ele} in Table 1); in addition, contribution of vdW interaction was also insignificant (−1.26 kcal/mol). Therefore, $\Delta\Delta G_{\text{ATP}\rightarrow\text{ADP}}$ was small, which showed good agreement with experimental data.

4. Conclusion

Homology modeling of catalytic NtpA subunit was performed to apply MD simulation/free energy calculation for *E. hirae* V-ATPase. The results obtained by MM-GBSA analysis of nucleotide binding affinity showed qualitatively good agreement with previously obtained experimental data and TI simulation provided quantitatively good corresponding values.

Our study is a novel approach to explain the difference of nucleotide binding properties in V-ATPase NtpA subunit. The overall result indicates that this can be a good first step toward the understanding of nucleotide binding to $NtpA_1B_1$ dimer, $NtpA_3B_3$ hexamer and to explore catalytic behavior by computer simulation at atomic level details.

Acknowledgements

We thank the RIKEN Integrated Cluster of Clusters (RICC) at RIKEN and "High performance computing system" at Tokyo University of Science (TUS) for the computer resources used for the calculation. This work was supported by grants-in-aid (23118705 and 23370047) from the Ministry of Education, Culture, Sports, Science and Technology of Japan.

Appendix A. Supplementary data

Supplementary data associated with this article can be found, in the online version, at http://dx.doi.org/10.1016/j.jmgm.2012.03.006.

References

[1] M. Forgac, Vacuolar ATPases: rotary proton pumps in physiology and pathophysiology, Nat. Rev. Mol. Cell. Biol. 8 (2007) 917–929.
[2] D.L. Heefner, F.M. Harold, ATP-driven sodium pump in *Streptococcus faecalis*, Proc. Natl. Acad. Sci. U.S.A. 79 (1982) 2798–2802.
[3] H. Imamura, K. Yokoyama, Two rotary molecular motors, V-ATPase and F_oF_1, Seikagaku 79 (2007) 425–437.
[4] J. Weber, A.E. Senior, Catalytic mechanism of F_1-ATPase, Biochim. Biophys. Acta 1319 (1997) 19–58.
[5] O. Panke, B. Rumberg, Kinetic modeling of rotary CF_oF_1-ATP synthase: storage of elastic energy during energy transduction, Biochim. Biophys. Acta 1412 (1999) 118–128.
[6] J.P. Abrahams, A.G. Leslie, R. Lutter, J.E. Walker, Structure at 2.8 A resolution of F_1-ATPase from bovine heart mitochondria, Nature 370 (1994) 621–628.
[7] H. Noji, R. Yasuda, M. Yoshida, K. Kinosita Jr., Direct observation of the rotation of F_1-ATPase, Nature 386 (1997) 299–302.
[8] H. Ren, W.S. Allison, On what makes the gamma subunit spin during ATP hydrolysis by F(1), Biochim. Biophys. Acta 1458 (2000) 221–233.
[9] W. Yang, Y.Q. Gao, Q. Cui, J. Ma, M. Karplus, The missing link between thermodynamics and structure in F_1-ATPase, Proc. Natl. Acad. Sci. U.S.A. 100 (2003) 874–879.
[10] Y.Q. Gao, W. Yang, R.A. Marcus, M. Karplus, A model for the cooperative free energy transduction and kinetics of ATP hydrolysis by F_1-ATPase, Proc. Natl. Acad. Sci. U.S.A. 100 (2003) 11339–11344.
[11] J. Pu, M. Karplus, How subunit coupling produces the gamma-subunit rotary motion in F_1-ATPase, Proc. Natl. Acad. Sci. U.S.A. 105 (2008) 1192–1197.
[12] Y.Q. Gao, W. Yang, M. Karplus, A structure-based model for the synthesis and hydrolysis of ATP by F_1-ATPase, Cell 123 (2005) 195–205.
[13] R.A. Bockmann, H. Grubmuller, Nanoseconds molecular dynamics simulation of primary mechanical energy transfer steps in F1-ATP synthase, Nat. Struct. Biol. 9 (2002) 198–202.
[14] T. Murata, M. Kawano, K. Igarashi, I. Yamato, Y. Kakinuma, Catalytic properties of Na(+)-translocating V-ATPase in *Enterococcus hirae*, Biochim. Biophys. Acta 1505 (2001) 75–81.
[15] K. Takase, I. Yamato, Y. Kakinuma, Cloning and sequencing of the genes coding for the A and B subunits of vacuolar-type Na(+)-ATPase from *Enterococcus hirae*. Coexistence of vacuolar- and F_oF_1-type ATPases in one bacterial cell, J. Biol. Chem. 268 (1993) 11610–11616.
[16] T. Hosaka, K. Takase, T. Murata, Y. Kakinuma, I. Yamato, Deletion analysis of the subunit genes of V-type Na^+-ATPase from *Enterococcus hirae*, J. Biochem. 139 (2006) 1045–1052.
[17] T. Murata, I. Yamato, Y. Kakinuma, M. Shirouzu, J.E. Walker, S. Yokoyama, S. Iwata, Ion binding and selectivity of the rotor ring of the Na^+-transporting V-ATPase, Proc. Natl. Acad. Sci. U.S.A. 105 (2008) 8607–8612.
[18] T. Murata, K. Takase, I. Yamato, K. Igarashi, Y. Kakinuma, Properties of the V_oV_1 Na^+-ATPase from *Enterococcus hirae* and its V_o moiety, J. Biochem. 125 (1999) 414–421.
[19] S. Arai, I. Yamato, A. Shiokawa, S. Saijo, Y. Kakinuma, Y. Ishizuka-Katsura, M. Toyama, T. Terada, M. Shirouzu, S. Yokoyama, S. Iwata, T. Murata, Reconstitution in vitro of the catalytic portion ($NtpA_3$-B_3-D-G complex) of *Enterococcus hirae* V-type Na^+-ATPase, Biochem. Biophys. Res. Commun. 390 (2009) 698–702.
[20] K. Takase, S. Kakinuma, I. Yamato, K. Konishi, K. Igarashi, Y. Kakinuma, Sequencing and characterization of the ntp gene cluster for vacuolar-type Na(+)-translocating ATPase of *Enterococcus hirae*, J. Biol. Chem. 269 (1994) 11037–11044.
[21] T. Murata, I. Yamato, Y. Kakinuma, Structure and mechanism of vacuolar Na^+-translocating ATPase from *Enterococcus hirae*, J. Bioenerg. Biomembr. 37 (2005) 411–413.
[22] T. Murata, I. Yamato, Y. Kakinuma, A.G. Leslie, J.E. Walker, Structure of the rotor of the V-Type Na^+-ATPase from *Enterococcus hirae*, Science 308 (2005) 654–659.
[23] M.S. Manimekalai, A. Kumar, J. Jeyakanthan, G. Gruber, The transition-like state and Pi entrance into the catalytic a subunit of the biological engine A-ATP synthase, J. Mol. Biol. 408 (2011) 736–754.
[24] A. Sali, Comparative protein modeling by satisfaction of spatial restraints, Mol. Med. Today 1 (1995) 270–277.
[25] G. Wu, D.H. Robertson, C.L. Brooks 3rd, M. Vieth, Detailed analysis of grid-based molecular docking: a case study of CDOCKER-A CHARMm-based MD docking algorithm, J. Comput. Chem. 24 (2003) 1549–1562.
[26] A. Jakalian, B.L. Bush, D.B. Jack, C.I. Bayly, Fast, efficient generation of high-quality atomic charges. AM1-BCC model: I. Method, J. Comput. Chem. 21 (2000) 132–146.
[27] W. Humphrey, A. Dalke, K. Schulten, VMD: visual molecular dynamics, J. Mol. Graph. 14 (1996), 33–38, 27–38.
[28] H.J.C. Berendsen, J.P.M. Postma, W.F. van Gunsteren, A. DiNola, J.R. Haak, Molecular-dynamics with coupling to an external bath, J. Chem. Phys. 81 (1984) 3684–3690.
[29] J.-P. Ryckaert, G. Ciccotti, H.J.C. Berendsen, Numerical integration of the cartesian equations of motion of a system with constraints: molecular dynamics of n-alkanes, J. Comput. Phys. 23 (1977) 327–341.
[30] D. Bashford, D.A. Case, Generalized born models of macromolecular solvation effects, Annu. Rev. Phys. Chem. 51 (2000) 129–152.
[31] H. Gouda, I.D. Kuntz, D.A. Case, P.A. Kollman, Free energy calculations for theophylline binding to an RNA aptamer: comparison of MM-PBSA and thermodynamic integration methods, Biopolymers 68 (2003) 16–34.

[32] M.J. Maher, S. Akimoto, M. Iwata, K. Nagata, Y. Hori, M. Yoshida, S. Yokoyama, S. Iwata, K. Yokoyama, Crystal structure of A_3B_3 complex of V-ATPase from *Thermus thermophilus*, EMBO J. 28 (2009) 3771–3779.
[33] A. Kumar, M.S. Manimekalai, A.M. Balakrishna, J. Jeyakanthan, G. Gruber, Nucleotide binding states of subunit A of the A-ATP synthase and the implication of P-loop switch in evolution, J. Mol. Biol. 396 (2010) 301–320.
[34] D.A. Pearlman, Evaluating the molecular mechanics poisson-boltzmann surface area free energy method using a congeneric series of ligands to p38 MAP kinase, J. Med. Chem. 48 (2005) 7796–7807.
[35] G. Hummer, A. Szabo, Calculation of free-energy differences from computer simulations of initial and final states, J. Chem. Phys. 105 (1996) 2004–2010.